

## **EFFECTS OF STEP POSITION ON THE AERODYNAMIC SURFACE QUANTITIES OF A RAREFIED HYPERSONIC FLOW OVER FORWARD-FACING STEPS**

**Paulo H. M. Leite**

*phmineiro@gmail.com*

*Brazilian Army, 2nd Jungle Infantry Brigade*

*São Gabriel da Cachoeira, AM, 69750-000 Brazil*

**Wilson F. N. Santos**

*wilson.santos@inpe.br*

*Combustion and Propulsion Laboratory (LCP), National Institute for Space Research (INPE)*

*Cachoeira Paulista, SP, 12630-000, Brazil*

**Abstract.** This work describes a computational analysis of a non-reacting hypersonic flow in thermal non-equilibrium over forward-facing steps at zero-degree angle of attack. Effects on the aerodynamic surface quantities due to changes on the step position have been investigated by employing the Direct Simulation Monte Carlo (DSMC) method. The work focuses the attention of designers of hypersonic configurations on the fundamental parameter of surface discontinuity, which can have an important impact on even initial design. Results highlight the sensitivity of the heat transfer, pressure, and skin friction coefficients due to changes on the step position for forward-facing step with different step height. The analysis showed that the upstream disturbance in the step configuration decreased with increasing the step position and increased with increasing the frontal-face height. In addition, it was found that pressure and heating loads decreased with increasing the step position and increased with increasing the step frontal face height.

**Keywords:** DSMC, Rarefied flow, Hypersonic flow, Forward-facing step, Aerodynamic heating.

## 1 Introduction

The study of separated and reattached supersonic flows has been an important area of fluid mechanics research in the last decades. These flows are frequent on surfaces of high-speed aerodynamic configurations, in which the performance may be degraded by separated flows, and various components damaged due to intense heating loads at reattachment. Included in these flows are shock-boundary layer interactions, wakes, as well as desired or undesired design features such as cavity, gap and step. For instance, the thermal protection system (TPS) of the Space Shuttle Orbiter requires gaps between the used protection elements to account for thermal expansion. In addition, in the case of reentry vehicles, the boundary layer transition prediction is a requirement to define the TPS. This protection is usually designed as an assembly of tiles. Gaps between tiles may modify the boundary-layer state and eventually promote transition, inducing higher temperature levels than those expected. Therefore, knowledge of heat transfer rates in separated flow regions would permit a more accurate analysis of associated heat transfer problems, as well as a more thorough understanding of flow separation.

There have been considerable studies on separated flow related to surface discontinuities [1, 2, 3, 4, 5, 6, 7, 8, 9, 10, 11, 12, 13, 14, 15, 16, 17, 18]. In general, these studies are devoted primarily to experimental and computational studies dealing with flows on protuberances, cavity, gap, forward- and backward-facing steps. For the purpose of this introduction, it will be sufficient to describe only a few of these studies.

Bertran and Wiggs [1] investigated experimentally the effect of distortions, consisting of small protuberances and holes, on the wing of a hypersonic vehicle. The effect on the pressure and on the heat flux to the surface was investigated for a range of Mach number from 7 to 10 and angle of attack up to 20 degrees. Results showed that these surface distortions presented a lower influence on the pressure rather than on the heat-flux distributions. They also showed that all distortions investigated caused an increase in the aerodynamic heating.

Rogers and Berry [2] conducted an experimental investigation on forward-facing steps in a supersonic flow,  $M_\infty \approx 2$ , characterized by a thick laminar boundary layer. Freestream pressure was defined at 30, 50 and 70  $\mu\text{mHg}$ , covering a Reynolds number per inch between 98 and 281. Eight step heights were tested, ranging in 0.1 inch intervals from 0.1 to 0.9 inches, except 0.8 inch. In addition, the step height was comparable with the local boundary-layer thickness for the flat-plate without steps. According to them, the investigation showed that the largest pressure rise occurred at the step face. Furthermore, it was found that this pressure rise depends on height-to-length ( $h/l$ ) ratio, where  $h$  is the step height and  $l$  is the distance from the flat-plate leading edge to the step.

By employing the DSMC method, Pullin and Harvey [4] analysed a two-dimensional (2-D) rarefied hypersonic flow around a forward-facing step by considering  $\text{N}_2$  as the working fluid, and a freestream Mach number of 22. The analysis showed that in the vicinity of the step base, the flow has a rapid deceleration and compression accompanied by a sudden transition to a near-continuum Navier-Stokes type state nearly in equilibrium at the body temperature. Their computational results presented good agreement with experimental data.

Bertin and Keisner [7] investigated experimentally the effect of a step and a gap tile misalignment on transition locations in the plane of symmetry of the Space Shuttle Orbiter. Data were obtained for a Mach number of 8 and angle of attack of 30 degrees. Data correlations, relating the location of the boundary-layer transition on the vehicle surface, were presented in the continuum flow regime. They concluded that the step height is more effective in the boundary-layer transition than the gap length.

Grotowsky and Ballmann [15] investigated laminar hypersonic flow over forward- and backward-facing steps by employing Navier-Stokes equations. The hypersonic flow over the steps were simulated by considering freestream Mach number of 8, Reynolds number of the order of  $10^5$  and an altitude of 30 km. According to them, the computational results presented a good agreement with the experimental data available in the literature. They also pointed out that the quantitative comparison exhibited major differences for the wall heat flux, probably due to the difficulty in how to measure accurately.

In general, the majority of the available research studies on cavities, gaps, and steps has been con-

ducted in order to understand, among others, the physical aspects of a laminar or turbulent boundary layer in a subsonic, supersonic or hypersonic flow past to these types of discontinuities, characterized by a sudden change on the surface slope. However, there is little understanding of the physical aspects of rarefied hypersonic flows past to these surface discontinuities related to the aerothermodynamic environment associated with a reentry vehicle.

In this scenario, Leite and Santos [19] have examined forward-facing steps situated in a rarefied hypersonic flow by employing the DSMC method. The study was motivated by the interest in examining the impact of the frontal-face heights on the flowfield structure and on the aerodynamic surface quantities in the transition flow regime, i.e., between the continuum flow and the free collision flow regime. The computational results showed that the step height changes contributed to significant modifications in the flowfield structure ahead the step. The analysis showed a significant increase in the primary flow properties in the vicinity of the step base. The aerodynamic surface quantities were directly influenced by the recirculation region ahead the step. Furthermore, high pressure and heat loads were observed in the vicinity of the step frontal face as a consequence of the recirculation region ahead the step.

In continuation of the surface discontinuity study, the present account extends further the previous analysis [19] by investigating the impact of the step position on the aerodynamic surface quantities for a hypersonic flow over a forward-facing step configuration. In this fashion, the prime concern of this study is to assess the sensitivity of the heat transfer, pressure, and skin friction coefficients due to changes on the step position for different step frontal-face height. Again, the DSMC method will be employed to calculate the 2-D hypersonic flow over the forward-facing steps.

## **2 Computational Method**

The DSMC method [20] is a standard method for simulation of rarefied flow with a significant degree of non-equilibrium. The DSMC method model a gas flow by using a computer to track the trajectory of simulated particles, where each simulated particle represents a fixed number of real gas particles. The movement and collision behavior of simulated particles within the flowfield are decoupled over a time step, which is a small fraction of the local mean collision time. For each time step, particle positions are deterministically updated according to their momentum. Boundary conditions are enforced, e.g. particles may interact with walls, they may be injected to or removed from the computed domain. In addition, collisions particles interact with each other on a probabilistic basis, and sampling macroscopic flow parameters are determined from both space and time averaged particle properties.

For the purpose to facilitate the choice of molecules for collisions and for the sampling of the macroscopic flow properties, the physical space is divided into regions, which are subdivided into computational cells. The cells are further subdivided into subcells. In order to guarantee a physically correct collision partner selection [21], the cell dimensions should be less than the local mean free path. If distance between a pair of colliding molecules is larger than the local mean free path, then there would be a physically incorrect transfer of momentum and energy. In addition, the DSMC method has no requirement that cells be regular and/or orthogonal.

In the present account, intermolecular collisions are treated by using the variable hard sphere (VHS) molecular model [22], and the no time counter (NTC) collision sampling technique [23]. The VHS model employs the simple hard sphere angular scattering law so that all directions are equally possible for post-collision velocity in the center-of-mass frame of reference. Nevertheless, the collision cross section depends on the relative speed of colliding molecules. Simulations are performed by using a non-reacting gas model, consisting of  $N_2$  and  $O_2$ , while considering energy exchange between translational, rotational and vibrational modes. Energy partitioning is accounted for using the Borgnakke-Larsen statistical model [24] with rotational and vibrational collision numbers for internal relaxation, obtained in a collision energy-based procedure as suggested by Boyd [25] for rotation and by Bird [26] for vibration. For a given collision, the probabilities are designated by the inverse of the relaxation numbers, which correspond to the number of collisions necessary, on average, for a molecule to reach thermal equilibrium.

### 3 Geometry Definition

In the present account, the forward-facing step is the same as that presented in Leite and Santos [19]. Leite and Santos [19] considered that the step frontal-face  $h$  is much smaller than the nose radius  $R$  of a reentry capsule, i.e.,  $h/R \ll 1$ , then the hypersonic flow over the step may be considered as a hypersonic flow over a flat plate with a forward-facing step. Figure 1 illustrates a schematic view of the model employed along with the important parameters.

According to Fig. 1,  $M_\infty$  represents the freestream Mach number,  $h$  the frontal-face height,  $l$  the step position, and  $D$  the total length of the flat plate. It was assumed a frontal-face height  $h$  of 3, 6, and 9 mm, which correspond to the dimensionless height  $H(= h/\lambda_\infty)$  of 3.23, 6.46, and 9.69, respectively, where  $\lambda_\infty$  is the freestream mean free path at an altitude of 70 km. In addition, it was assumed the step position  $L(= l/\lambda_\infty)$  of 40, 50, and 60. As a result,  $D/\lambda_\infty$  correspond to 90, 100, and 110, respectively.

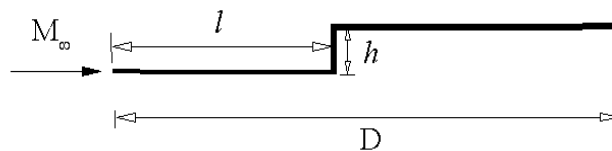


Figure 1. Drawing illustrating a schematic view of the forward-facing step configuration.

### 4 Freestream and Flow Conditions

Freestream flow conditions used for the numerical simulations are those given by Leite and Santos [19] and summarized in Tab. 1. Freestream conditions represent those experienced by a capsule at an altitude of 70 km. This altitude is associated with the rarefied flow regime, which is characterized by the overall Knudsen number the order of or larger than  $10^{-2}$ . Referring to Tab. 1,  $U_\infty$ ,  $T_\infty$ ,  $p_\infty$ ,  $\rho_\infty$ ,  $\mu_\infty$ ,  $n_\infty$ , and  $\lambda_\infty$  stand, respectively, for velocity, temperature, pressure, density, viscosity, number density, and molecular mean free path. Gas properties associated with the working fluid,  $N_2$  and  $O_2$ , such as mass fraction,  $\chi$ , molecular mass,  $m$ , molecular diameter,  $d$ , and viscosity index,  $\omega$ , are given by Bird [20] and summarized in Tab. 2.

The freestream velocity  $U_\infty$ , assumed to be constant at 7546 m/s, corresponds to a freestream Mach number  $M_\infty$  of 25. The wall temperature  $T_w$  is fixed at 880 K. This temperature is chosen to be representative of the surface temperature near the stagnation point of a reentry capsule, and it is assumed to be uniform on the step surface. As was mentioned by Leite and Santos [19], this surface temperature is low compared to the freestream stagnation temperature. This assumption seems reasonable since practical surface material will probably be destroyed if surface temperature is allowed to approach the stagnation

Table 1. Freestream flow conditions [19]

$U_\infty$ (m/s)	$T_\infty$ (K)	$p_\infty$ (N/m <sup>2</sup> )	$\rho_\infty$ (kg/m <sup>3</sup> )	$\mu_\infty$ (Ns/m <sup>2</sup> )	$n_\infty$ (m <sup>-3</sup> )	$\lambda_\infty$ (m)
7546	219.69	5.582	$8.753 \times 10^{-5}$	$1.455 \times 10^{-5}$	$1.8192 \times 10^{21}$	$9.285 \times 10^{-4}$

Table 2. Gas properties [20]

	$\chi$	$m$ (kg)	$d$ (m)	$\omega$
$O_2$	0.237	$5.312 \times 10^{-26}$	$4.07 \times 10^{-10}$	0.77
$N_2$	0.763	$4.650 \times 10^{-26}$	$4.17 \times 10^{-10}$	0.74

temperature. For the present account, the ratio of surface temperature to the stagnation temperature is around 0.032.

By assuming the step frontal-face height  $h$  as the characteristic length, the Knudsen number  $Kn_h$ , defined by the ratio of the mean free path in the freestream gas to the step height, corresponds to 0.3095, 0.1548 and 0.1032 for step height  $h$  of 3, 6 and 9 mm, respectively. Finally, the Reynolds number  $Re_h$ , also based on the frontal-face height  $h$  and on conditions in the undisturbed stream, is around 136, 272, and 409 for step height  $h$  of 3, 6 and 9 mm, respectively.

## 5 Computational Domain and Grid

The computational domain used for the simulation is made large enough so that disturbances from the step configuration do not reach the upstream and side boundaries, where freestream conditions are specified. The computational domain is divided into ten regions, which are subdivided into computational cells. The cells are further subdivided into subcells, two subcells/cell in each coordinate direction. A schematic view of the computational domain is demonstrated in Fig. 2.

Based on Fig. 2, side I-A is defined by the forward-facing step surface. Diffuse reflection with complete thermal accommodation was defined as the condition applied to this side. Therefore, molecules are reflected equally in all directions, and the final velocity of the molecules is randomly assigned according to a half-range Maxwellian distribution determined by the wall temperature  $T_w$ . In addition, the internal energies, rotation and vibration, of the molecules are also sampled from the appropriate equilibrium distribution by using the wall temperature  $T_w$ . Side I-B represents a plane of symmetry, where all flow gradients normal to the plane are zero. At the molecular level, this plane is equivalent to a specular reflecting boundary. Therefore, the only change to the properties of the molecules is the velocity component normal to the surface that is simply reversed in sign. Sides II and III are the freestream sides through which simulated molecules enter and exit. Side II is positioned at  $5\lambda_\infty$  upstream of the flat-plate leading edge, and side III defined at  $30\lambda_\infty$ ,  $34\lambda_\infty$ , and  $42\lambda_\infty$  above the upper surface for frontal-face height  $H$

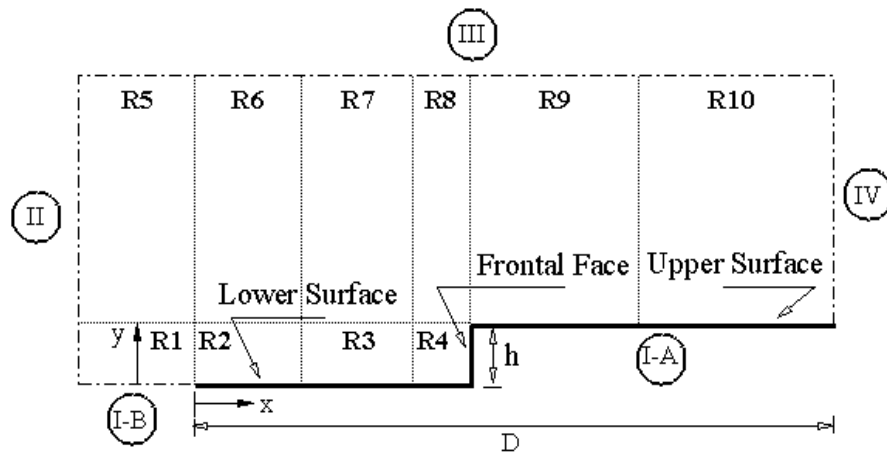


Figure 2. Drawing illustrating a schematic view of the computational domain.

Table 3. Region dimensions ( $x/\lambda_\infty \times y/\lambda_\infty$ ) and number of cells [ $x \times y$ ] for the  $L = 50$  case, and step height  $H$  of 3.23, 6.46, and 9.69.

	$H = 3.23$	$H = 6.46$	$H = 9.69$
<b>R1</b>	(5 × 3.23)[10 × 10]	(5 × 6.46)[10 × 20]	(5 × 9.69)[10 × 30]
<b>R2</b>	(20 × 3.23)[40 × 30]	(20 × 6.46)[40 × 50]	(20 × 9.69)[40 × 60]
<b>R3</b>	(20 × 3.23)[40 × 30]	(20 × 6.46)[40 × 50]	(20 × 9.69)[60 × 60]
<b>R4</b>	(10 × 3.23)[60 × 70]	(10 × 6.46)[110 × 120]	(10 × 9.69)[120 × 140]
<b>R5</b>	(5 × 30)[10 × 40]	(5 × 34)[10 × 50]	(5 × 42)[10 × 60]
<b>R6</b>	(20 × 30)[30 × 40]	(20 × 34)[30 × 50]	(20 × 42)[30 × 60]
<b>R7</b>	(20 × 30)[30 × 40]	(20 × 34)[30 × 50]	(20 × 42)[30 × 60]
<b>R8</b>	(10 × 30)[30 × 50]	(10 × 34)[30 × 60]	(10 × 42)[30 × 80]
<b>R9</b>	(25 × 30)[60 × 70]	(25 × 34)[70 × 90]	(25 × 42)[70 × 90]
<b>R10</b>	(25 × 30)[60 × 80]	(25 × 34)[60 × 80]	(25 × 42)[70 × 80]
<b># cells</b>	20,000	33,800	41,600

of 3.23, 6.46, and 9.69, respectively. Finally, the flow at the downstream outflow boundary, side IV, is predominantly supersonic and vacuum condition is specified [20]. Basically, at this boundary, simulated molecules can only exit. Nevertheless, it is important to mention that, close to the wall, molecules may not be moving at supersonic speed. As a result, in this subsonic region close to the wall, there is an interaction between the flow and the downstream boundary. However, the extent of the upstream effect of this boundary condition can be determined by changing the length of the upper surface. For the conditions investigated in the present work, the upstream disturbance [19] is approximately of  $6\lambda_\infty$ .

Numerical accuracy of the DSMC method depends on the cell size [27, 28], on the number of particles per computational cell [29, 30, 31], as well as on the time step [32, 33]. These effects were investigated to determine the number of cells and the number of particles required to achieve grid independence solutions. A grid independence study was made with three different groups of structured meshes – coarse, standard and fine – in each coordinate direction. The impact of altering the cell size in both coordinate directions,  $x$  and  $y$ , was investigated for a coarse and fine grids with, respectively, 50% fewer and 100% more cells with respect to the standard grid. In addition, each grid was made up of non-uniform cell spacing in both directions. Moreover, point clustering is used close to solid walls. Table 3 summarizes the main characteristics for the standard grid related to ten regions (R1 to R10 in Fig. 2) for the  $L = 50$  case and frontal-face height  $H$  of 3.23, 6.46, and 9.69.

The effect (not shown) on the heat transfer, pressure, and skin friction coefficients due to changes in the cell size in both directions was rather insensitive to the range of cell spacing considered, indicating that the standard grid, with the total number of cells shown in Tab. 3 is essentially grid independent.

A similar examination was made for the number of simulated molecules. The standard grid for the  $L = 50$  case corresponds to a total of 20,000, 33,800, and 41,600 molecules for frontal-face height  $H$  of 3.23, 6.46, and 9.69, respectively. New cases corresponding to 50% fewer and 100% more simulated molecules were investigated by using the same standard grid. As these cases presented the same results (not shown) for the heat transfer, pressure, and skin friction coefficients, hence the standard grids with a total of 20,000, 33,800, and 41,600 simulated molecules for frontal-face height  $H$  of 3.23, 6.46, and 9.69, respectively, are considered enough for the computation of the aerodynamic surface quantities.

A discussion of the verification process, i.e., the effects of the cell size, the number of simulated particles per cell, and time step on the aerodynamic surface quantities for the forward-facing steps presented herein along with the validation process is described in detail by Leite and Santos [19].

## 6 Computational Results and Discussion

It is the purpose of this section to compare and to discuss some differences in the aerodynamic surface quantities due to variations on the step position of a forward-facing step configuration for different frontal-face height. Surface quantities of particular interest in the present work are number flux,  $N$ , wall pressure,  $p_w$ , shear stress,  $\tau_w$ , and heat flux,  $q_w$ . These quantities,  $N$ ,  $p_w$ ,  $\tau_w$ , and  $q_w$ , expressed in dimensionless form, are given in the following subsections.

Before proceeding with the analysis, it is instructive to first examine the thickness of the boundary-layer,  $\delta$ , for the flat-plate case, without a step, employed as a benchmark in this investigation. The boundary-layer thickness was obtained by considering the condition  $u/U_\infty = 0.99$ , where  $u$  is the tangential velocity, i.e., the velocity component in the  $x$ -direction. For the corresponding step position,  $L$  of 40, 50, and 60, the flat-plate boundary-layer thickness,  $\delta/\lambda_\infty$ , is 15.20, 16.62, and 19.63, respectively. Consequently, the boundary-layer thickness is larger than the step frontal-face height investigated ( $h/\lambda_\infty$  of 3.23, 6.46, and 9.69), a flow feature of particular interest in this study.

It is important to mention that rarefied hypersonic flows are characterized by thick laminar boundary layers. In addition, the frontal-face height of the steps on the surface of hypersonic vehicles may be less than the boundary-layer thickness. Therefore, at the step position, the ratio,  $h/\delta$ , step height to boundary-layer thickness, is low and changes with increasing the step position.

### 6.1 Number Flux

In the DSMC code, the number flux,  $N$ , is calculated by sampling the molecules impinging on the surface by unit time and unit area. The distribution of the number flux along the step surfaces – lower, frontal face, and upper – is illustrated in Fig. 3, parameterized by the dimensionless step height  $H$  and position  $L$ . In this set of plots,  $N_f$  represents the number flux  $N$  normalized by  $n_\infty U_\infty$ , where  $n_\infty$  and  $U_\infty$  correspond, respectively, to the freestream number density and freestream velocity. In addition, left-column plots correspond to the number flux along lower and upper surfaces, and right-column plots refer to the number flux along the frontal-face surface. Also,  $X$  and  $Y$  stand, respectively, for the length  $x$  and the height  $y$  normalized by the freestream mean free path  $\lambda_\infty$ . As a basis of comparison, the dimensionless number flux  $N_f$  for the flat-plate case is also illustrated in Fig. 3. It is important to remark that the flat-plate case corresponds to a flat plate without a forward-facing step, i.e. it represents a smooth surface.

Looking first at the plots on left column of Fig. 3, it is clearly noticed that the number flux to the surface depends on the step position  $L$  and on the frontal-face height  $H$ . Close to the sharp leading edge, the behavior of the number flux to the step lower surface is similar to that for the flat-plate case. This is an expected behavior since the flow in this region is not affected by the presence of the step. As the flow develops downstream along the lower surface, the presence of the step is felt in the number flux distribution at section  $X$  that corresponds to the interaction point. In addition, this interaction point depends on the step position  $L$  as well as on the step frontal-face height  $H$ . From this section up to the section where the steps are located, the number flux to the lower surface dramatically increases in comparison to the number flux observed for the flat-plate case. It is seen that the peak value for the number flux decreases with increasing the step position  $L$  and increases with increasing the step height  $H$ . This significant increase in the number flux at the step base is directly related to the recirculation region that forms ahead of the step frontal face. The recirculation region concentrates a large number of molecules. The molecules enclosed in this region, when colliding with the lower and frontal-face surfaces, increase not only the number flux to both surfaces but also increase the heat flux, as shown in subsequent subsection.

Still referring to the plots on left column of Fig. 3, it is also noticed that, along upper surface, the number flux distribution is similar one to each other for the step position investigated. The number flux  $N_f$  presents high values in the vicinity of the step convex corner and then it approaches the flat-plate case values downstream along the surface for the step height investigated.

Turning next to the plots on right column of Fig. 3, it is observed that the number flux to the frontal-

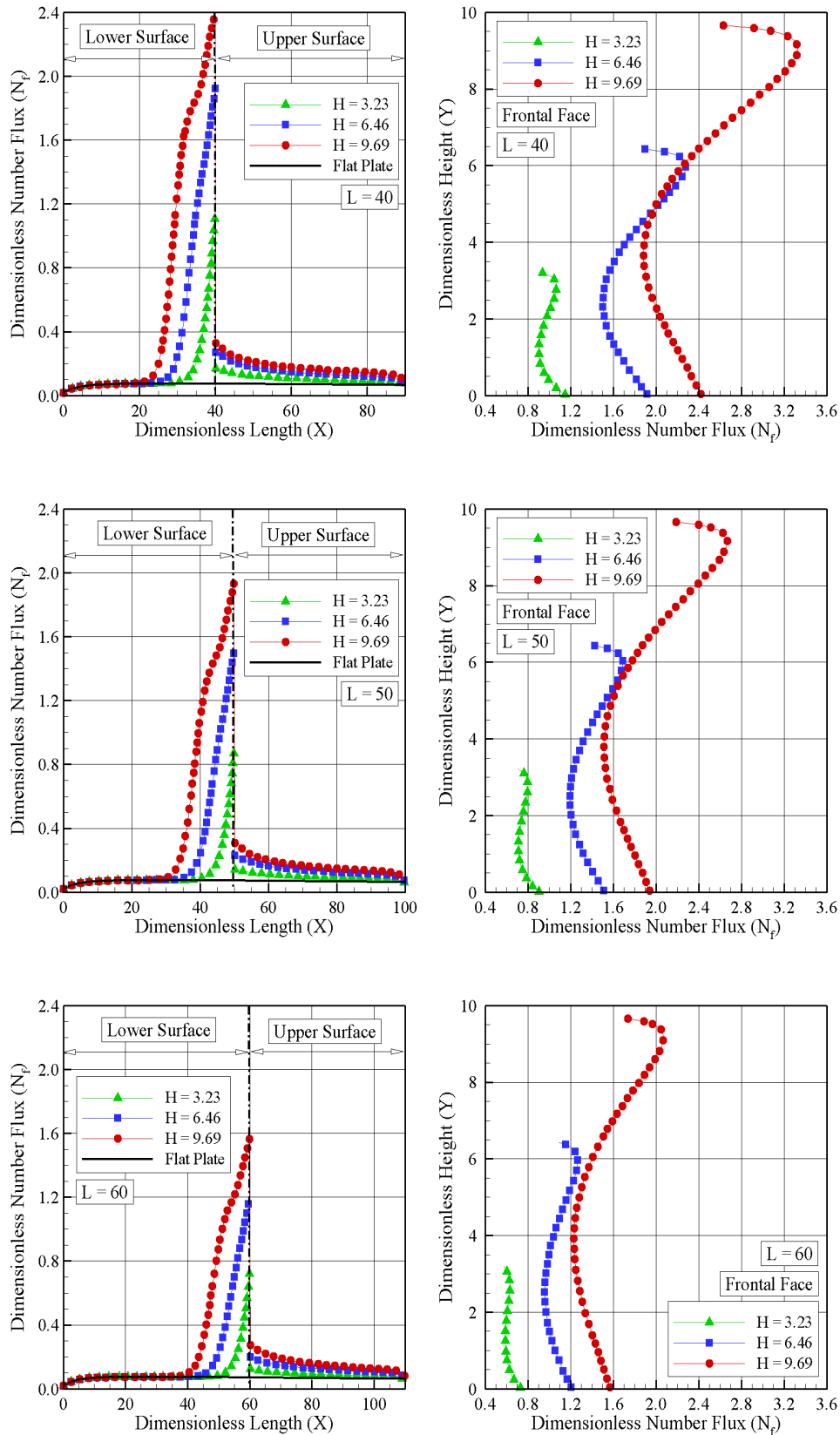


Figure 3. Distribution of dimensionless number flux  $N_f$  along lower and upper surfaces (left column) and frontal-face surface (right column) for dimensionless step position  $L$  of 40, 50, and 60.

face surface is more intense than that observed to the lower surface. Similar to that for the lower surface, the number flux to the frontal face is a function of the step position  $L$  and the step height  $H$ , i.e., it decreases with increasing the step position and it increases with the frontal-face height rise. It may be recognized from these plots that the number flux distribution presents a peak value in the vicinity of the step convex corner, except for the frontal-face height  $H = 3.23$ , where the pick values take place at the step base. This behavior is directly related to the large number of molecules in the recirculation region that forms ahead of the step frontal face. As a base of comparison, for the  $L = 50$  case, the peak value in the vicinity of the step convex corner takes place at section  $Y$  equal to 2.79, 5.03, and 9.16 for  $H$  of 3.23, 6.46, and 9.69, respectively. As a matter of fact, the flow reattachment point [19],  $Y_r$ , on the frontal face occurs for section  $Y$  equal to 2.72, 5.61 and 8.66 for  $H$  of 3.23, 6.46, and 9.69, respectively.

## 6.2 Pressure Coefficient

The pressure coefficient  $C_p$  is defined as follows,

$$C_p = \frac{p_w - p_\infty}{\frac{1}{2}\rho_\infty U_\infty^2} \quad (1)$$

where  $p_w$  is the wall pressure.

The pressure  $p_w$  on the body surface is calculated by the sum of the normal momentum fluxes of both incident and reflected molecules at each time step as follows,

$$p_w = p_i - p_r = \frac{F_N}{A\Delta t} \sum_{j=1}^N \{[(mv)_j]_i - [(mv)_j]_r\} \quad (2)$$

where  $F_N$  is the number of real molecules represented by a single simulated molecule,  $\Delta t$  is the time step,  $A$  the area,  $N$  is the number of molecules colliding with surface by unit time and unit area,  $v$  is the velocity component of the molecule  $j$  in the surface normal direction, and subscripts  $i$  and  $r$  refer to incident and reflect molecules.

The effect on the pressure coefficient  $C_p$  due to variation on the step position  $L$  and on the step height  $H$  is depicted in Fig. 4 for lower, frontal face, and upper surfaces. Again, in this set of plots,  $X$  and  $Y$  stand, respectively, for the length  $x$  and the height  $y$  normalized by the freestream mean free path  $\lambda_\infty$ . In addition, left-column plots correspond to the pressure coefficient  $C_p$  along lower and upper surfaces, and right-column plots,  $C_p$  along the frontal-face surface.

Referring to the plots on left column of Fig. 4, it is observed that the pressure coefficient  $C_p$  follows the same trend as that presented by the dimensionless number flux  $N_f$  in the sense that, along lower surface, the pressure coefficient  $C_p$  displays the same behavior as that for the flat-plate case up to the corresponding interaction point. In the vicinity of the step face, the pressure coefficient to lower surface increases in comparison to the pressure coefficient observed for the flat-plate case. In addition, similar to the number flux behavior, the pressure coefficient decreases with increasing the step position  $L$  and increases with increasing the step height  $H$ .

According to the plots on right column of Fig. 4, it is clearly seen that the pressure coefficient  $C_p$  follows the same behavior as that shown for the dimensionless number flux  $N_f$ , since the maximum values for  $C_p$  decreases by increasing the step position  $L$  and increases by increasing the step frontal face  $H$ . Again, peak values take place in the vicinity of the step convex corner. In addition, it is also observed that peak values on the step frontal face are larger than those on lower surface. For comparison purpose, for the  $L = 50$  case, the maximum values for  $C_p$  on the frontal face are around 0.61, 1.06 and 1.51 for height  $H$  of 3.23, 6.46 and 9.69, respectively. In contrast, the maximum value of  $C_p$  for the flat-plate case, i.e., a flat plate without steps, is around 0.0471 at section  $X = 25.57$  in the lower surface. Therefore,  $C_p$  of 0.61, 1.06 and 1.51 correspond respectively to 12.95, 22.52 and 32.06 times the peak value for the flat-plate case, which corresponds to a smooth surface.

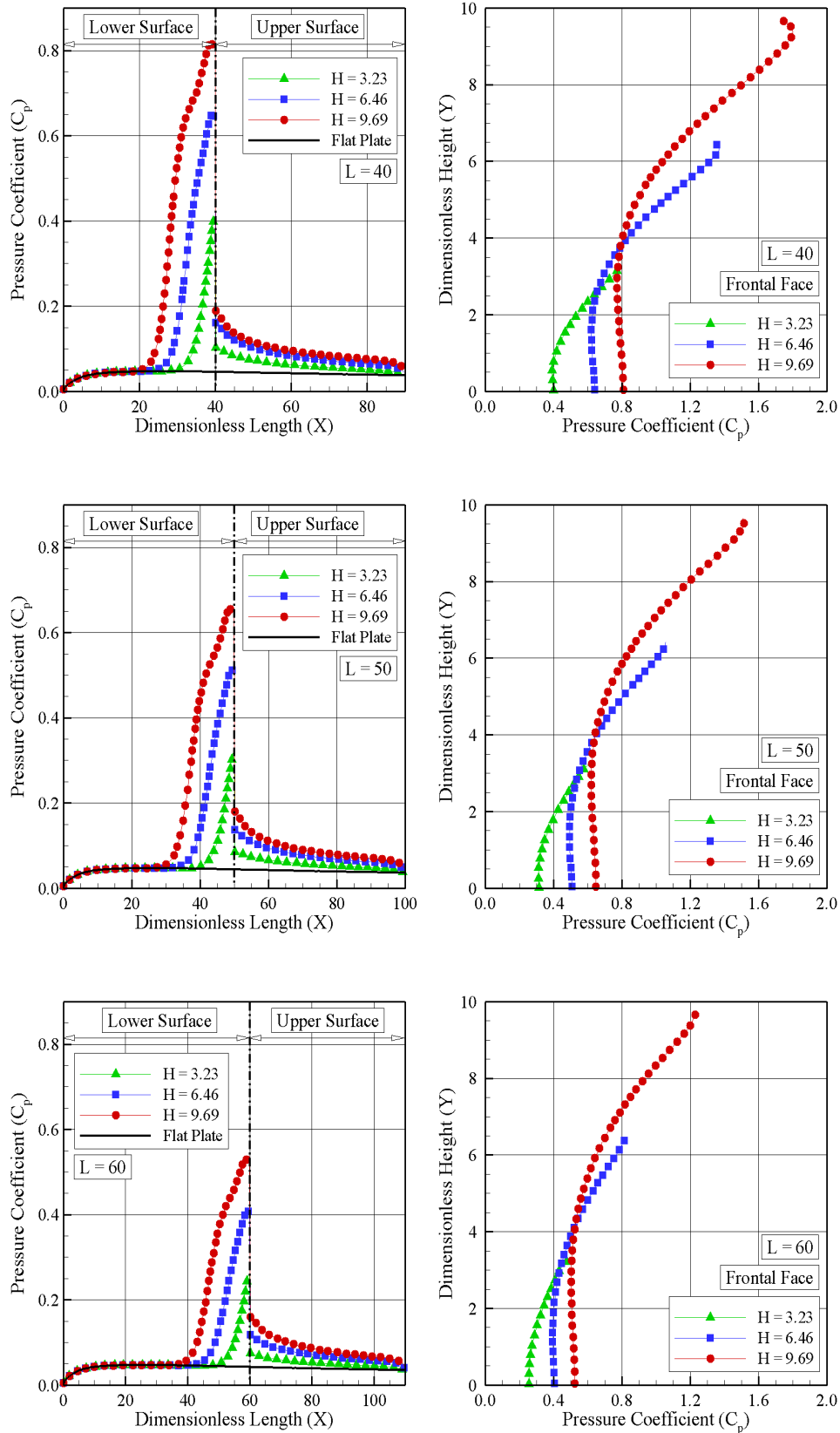


Figure 4. Distribution of pressure coefficient  $C_p$  along lower and upper surfaces (left column) and frontal-face surface (right column) for dimensionless step position  $L$  of 40, 50, and 60.

### 6.3 Skin Friction Coefficient

The skin friction coefficient  $C_f$  is defined as follows,

$$C_f = \frac{\tau_w}{\frac{1}{2}\rho_\infty U_\infty^2} \quad (3)$$

where  $\tau_w$  is the shear stress.

The shear stress  $\tau_w$  on the body surface is calculated by the sum of the tangential momentum fluxes of both incident and reflected molecules impinging on the surface at each time step by the following expression,

$$\tau_w = \tau_i - \tau_r = \frac{F_N}{A\Delta t} \sum_{j=1}^N \{[(mu)_j]_i - [(mu)_j]_r\} \quad (4)$$

where  $u$  is the velocity component of the molecule  $j$  in the surface tangential direction.

However, for diffuse reflection, the reflected molecules have a tangential moment equal to zero, since the molecules essentially lose, on average, their tangential velocity components. In this fashion, the contribution of  $\tau_r$  in Eq. 4 is equal to zero.

The impact on the skin friction coefficient  $C_f$  due to changes on the step position  $L$  and on step height  $H$  is demonstrated in Fig. 5, for lower, frontal face, and upper surfaces. According to the plots on the left column of Fig. 5, it is observed that the upstream disturbances, due to the presence of the step frontal face, are felt in the skin friction coefficient  $C_f$  close to the interaction point. From this point up to the step position, the skin friction coefficient  $C_f$  decreases, when compared to that for the flat-plate case, and reaches zero at section  $X$  that relies not only on the step position  $L$  but also on the step height  $H$ . After that, as a result of the recirculation region, the skin friction coefficient  $C_f$  continues to decrease up to a minimum point. After the minimum point,  $C_f$  increases again and reaches positive values at the base of the step.

It should be mentioned in this context that the separation point  $x_s$  on lower surface and the reattachment point  $y_r$  on the step frontal face were obtained on the basis of zero skin friction coefficient,  $C_f = 0$  (or wall shear stress  $\tau_w = 0$ ). The reason for that is because the skin friction coefficient along a surface usually changes from positive value to negative value at separation and vice-versa at reattachment in a 2-D flow, as pointed out by Kim and Setoguchi [34] and Deepak et al. [35]. Therefore, it is a good indication of the position of separation on lower surface and reattachment at the step frontal face. As a base of comparison, Tab. 4 presents the reattachment point  $y_r$ , normalized by the step height  $h$ , on the frontal-face surface for the cases investigated. It is seen that, as normalized by the step height  $h$ , the reattachment point slightly increases with the step height. Nevertheless, no significant changes are observed in the reattachment point by increasing the step position  $L$ , for the conditions investigated.

Along upper surface, similar to the pressure coefficient, it is noticed that the skin friction coefficient  $C_f$  is larger than that for the flat-plate case, especially in the vicinity of the step convex corner. However, as the flow moves downstream along the surface, the skin friction coefficient  $C_f$  basically tends to the value observed for the flat-plate case. Finally, it may be observed that the peak values for the skin friction coefficient  $C_f$  along upper surface are larger than those observed for the pressure coefficient. As a result, tangential forces, associated to the shear stress, are larger than normal forces, related to the wall pressure.

Table 4. Reattachment point  $y_r/h$ .

	$H = 3.23$	$H = 6.46$	$H = 9.69$
$L = 40$	0.831	0.866	0.878
$L = 50$	0.842	0.868	0.893
$L = 60$	0.845	0.870	0.902

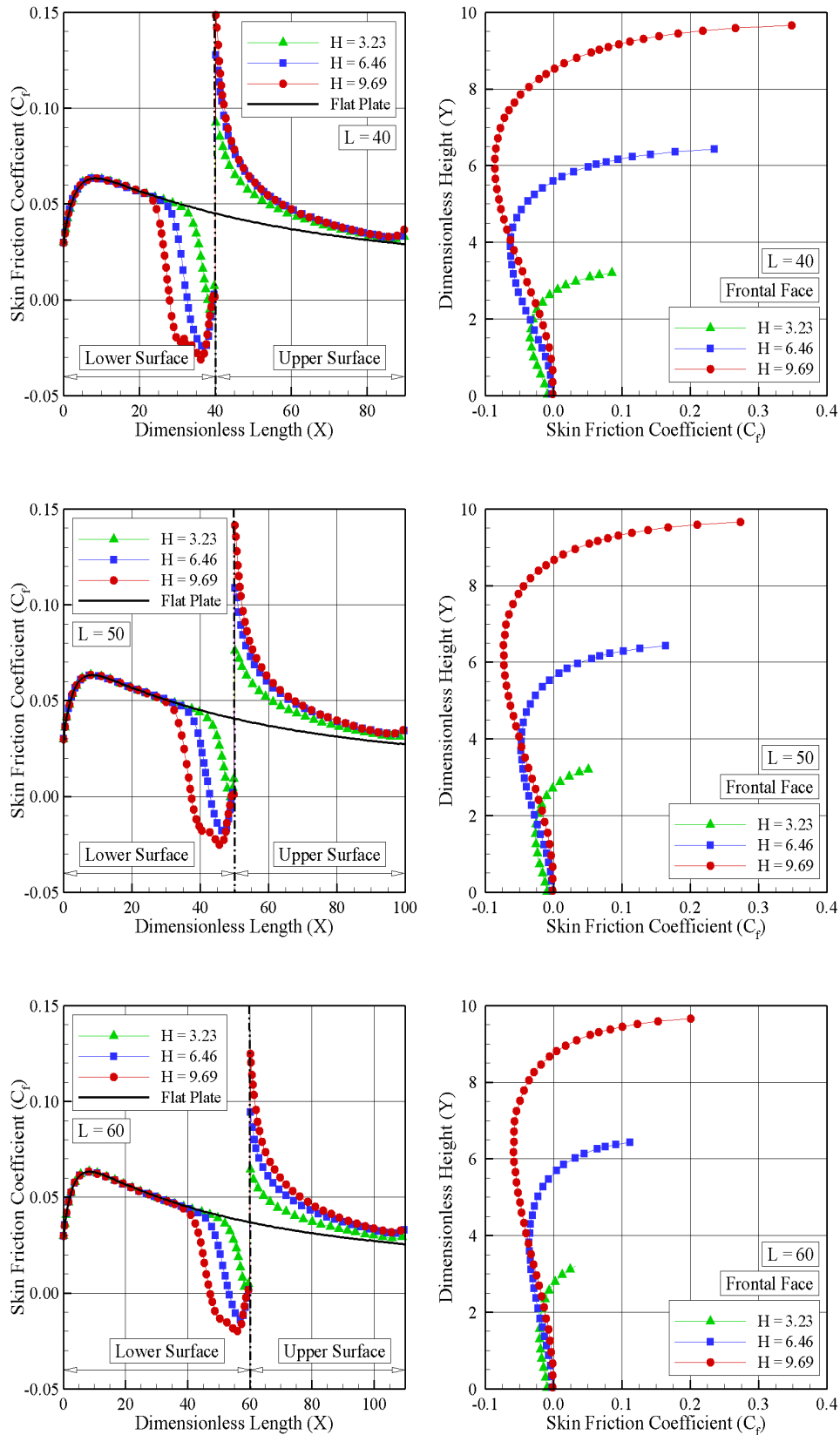


Figure 5. Distribution of skin friction coefficient  $C_f$  along lower and upper surfaces (left column) and frontal-face surface (right column) for dimensionless step position  $L$  of 40, 50, and 60.

## 6.4 Heat Transfer Coefficient

The heat transfer coefficient  $C_h$  is defined as follows,

$$C_h = \frac{q_w}{\frac{1}{2}\rho_\infty U_\infty^3} \quad (5)$$

where  $q_w$  is the heat flux to the body surface

The heat flux  $q_w$  is calculated by the net energy flux of the molecules impinging on the surface. A flux is regarded as positive if it is directed toward the body surface. The net heat flux  $q_w$  is related to the sum of the translational, rotational and vibrational energies of both incident and reflected molecules as defined by,

$$q_w = q_i - q_r = \frac{F_N}{A\Delta t} \left\{ \sum_{j=1}^N \left[ \frac{1}{2} m_j c_j^2 + e_{Rj} + e_{Vj} \right]_i - \sum_{j=1}^N \left[ \frac{1}{2} m_j c_j^2 + e_{Rj} + e_{Vj} \right]_r \right\} \quad (6)$$

where  $m$  is the mass of the molecules,  $c$  is the velocity of the molecules,  $e_R$  and  $e_V$  stand for rotational and vibrational energies, respectively.

The sensitivity of the heat transfer coefficient  $C_h$  is demonstrated in Fig. 6 for lower, frontal face, and upper surfaces. According to this group of plots, important features can be observed in the heat transfer coefficient behavior. It is seen that, similar to the number flux, the heat transfer coefficient  $C_h$  for forward-facing steps follows the same behavior presented by the flat-plate case close to the sharp leading edge, i.e., the region unaffected by the presence of the steps. In addition, further downstream along the lower surface, the heat transfer coefficient  $C_h$  significantly increases and reaches peak values close to the frontal face, then decreases to almost zero at the stagnation region. Along the upper surface, the heat transfer coefficient presents a maximum value at the step convex corner and then decreases downstream along the surface, basically approaching the values observed for the flat-plate case. Along the frontal face, the heat transfer coefficient  $C_h$  increases monotonically, from zero at the stagnation point to a maximum value near the step convex corner, which depends on the frontal-face height  $H$  and on the step position  $L$ . It is quite apparent that this significant increase in the heat transfer coefficient is due to the flow reattachment zone. It is also seen that the maximum values observed for the heat transfer coefficient  $C_h$  on the frontal-face surface is an order of magnitude larger than those observed on the lower surface.

For comparative purpose, Tab. 5 tabulates the maximum values for the heat transfer coefficient  $C_h$  in the frontal-face surface for the cases investigated. Therefore, the heat transfer coefficient  $C_h$  increases with the step height  $H$  and decreases with increasing the step position  $L$ . For instance, for the  $L = 40$  case, the maximum values for  $C_h$  are around 0.259, 0.427 and 0.529 for height  $H$  of 3.23, 6.46 and 9.69, respectively. In contrast, the  $C_h$  for the flat-plate case, i.e., a flat plate without steps, is around 0.031 at section  $X = 8.62$  in the lower surface. Therefore,  $C_h$  of 0.259, 0.427 and 0.529 correspond respectively to 8.35, 13.77 and 17.06 times the peak value for the flat-plate case.

Table 5. Maximum values for the heat transfer coefficient  $C_h$  at the frontal-face surface.

	$H = 3.23$	$H = 6.46$	$H = 9.69$
$L = 40$	0.259	0.427	0.529
$L = 50$	0.202	0.336	0.468
$L = 60$	0.152	0.268	0.385

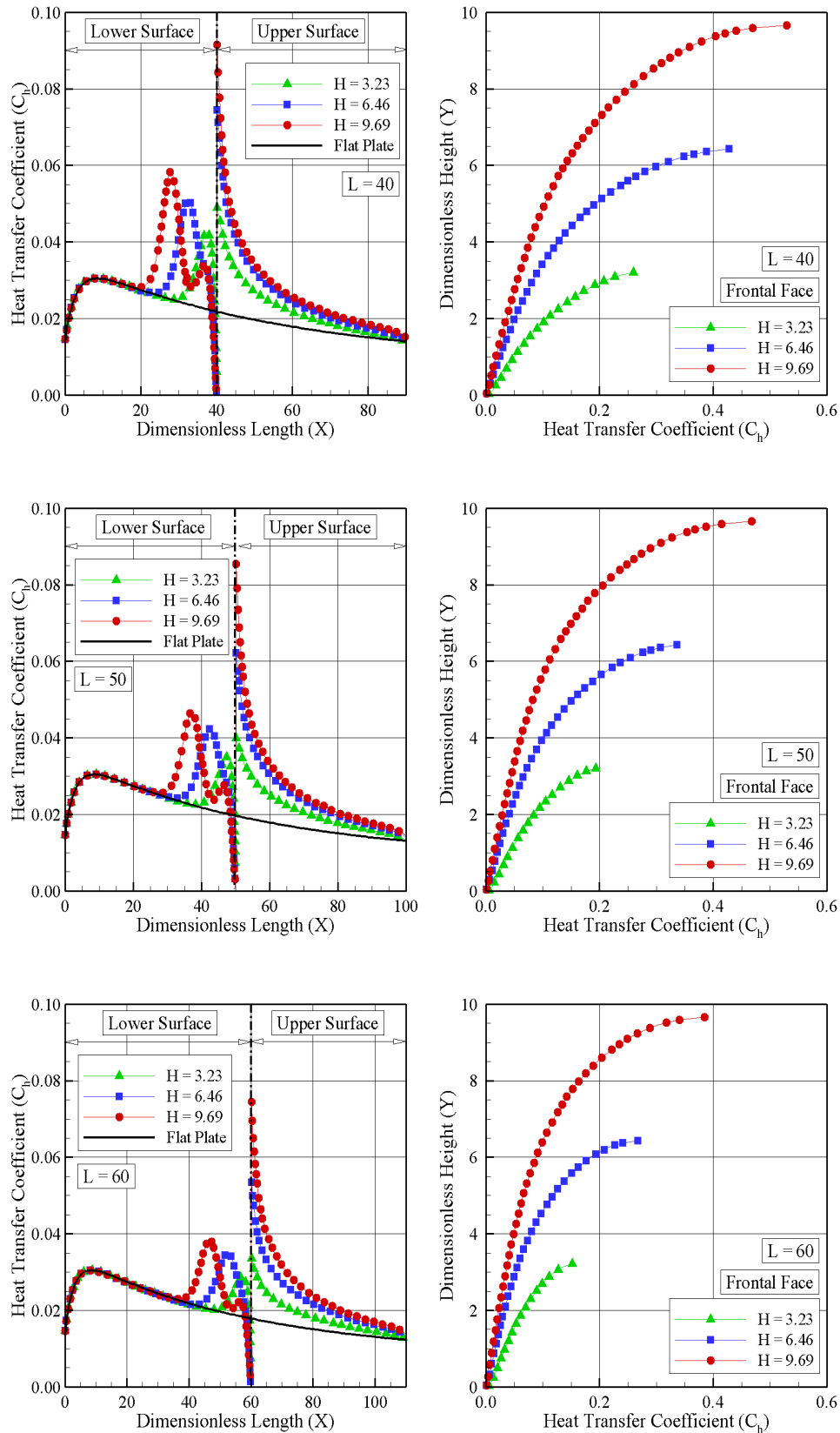


Figure 6. Distribution of heat transfer coefficient  $C_h$  along lower and upper surfaces (left column) and frontal-face surface (right column) for dimensionless step position  $L$  of 40, 50, and 60.

## 7 Concluding Remarks

A detailed numerical study has been carried out to investigate a rarefied hypersonic flow over a forward-facing step by using the Direct Simulation Monte Carlo (DSMC) method. The simulations provided information about the aerodynamic properties on the surfaces of the step configuration. Effects of the step position on the number flux, pressure, skin friction, and heat transfer coefficients were investigated for a representative range of parameters. The step position ranged from  $40\lambda_\infty$  to  $60\lambda_\infty$ , and the step frontal-face height  $h$  ranged from  $3.23\lambda_\infty$  to  $9.69\lambda_\infty$ , which corresponded, respectively, to Knudsen number  $Kn_h$  from 0.3095 to 0.1032, and Reynolds number  $Re_h$  from 136 to 409.

The analysis showed that changes on the step position and on the step frontal face thickness affected the heating and pressure loads, on the upstream surface and on the frontal face, for the range of parameters investigated. It was also found that heating rate and pressure load decreased with increasing the step position and increased with increasing the step frontal face. It was found that these loads exhibited maximum values on the step face, more precisely in the vicinity of the step shoulder. In addition, these loads are much higher than the maximum values found for a smooth surface, i.e., a flat plate without a forward-facing step. Consequently, in a hypersonic vehicle design, heating and pressure loads become important if discontinuities, such as a step, are present in the vehicle surface.

## Acknowledgements

The author (W. F. N. Santos) would like to thank the financial support provided by CNPq (Conselho Nacional de Desenvolvimento Científico e Tecnológico) under Grant No. 308832/2018-3.

## References

- [1] Bertran, M. H., & Wiggs, M. M., 1963. Effect of surface distortions on the heat transfer to a wing at hypersonic speeds. *AIAA Journal*, vol. 1, pp. 1313–1319.
- [2] Rogers, E. W. E., & Berry, C. J., 1965. Research at the NPL on the influence at supersonic speeds and low Reynolds numbers of thick laminar boundary layers. In: *Advances in Applied Mechanics: Rarefied Gas Dynamics*, I, Suppl. 3, pp. 574–591, Academic Press, New York.
- [3] Weinstein, I., Avery, D. E., & Chapman, A. J., 1975. Aerodynamic heating to gaps and surfaces of simulated reusable-surface-insulation tile arrays in turbulent flow at Mach 6.6. NASA TM X-3225.
- [4] Pullin, D. I., & Harvey, J. K., 1977. Direct simulation calculations of the rarefied flow past a forward-facing step. *AIAA Journal*, vol. 15, pp. 124–126.
- [5] Wieting, A. R., 1978. Experimental investigation of heat-transfer distributions in deep cavities in hypersonic separated flow. NASA TN D-5908.
- [6] Avery, D. E., 1978. Aerodynamic heating in gaps of thermal protection system tile arrays in laminar and turbulent boundary layers. NASA TP 1187.
- [7] Bertin, J. J., & Keisner, A., 1978. Effect of step and/or gap tile misalignment on shuttle transition. NASA-CR-151833.
- [8] Scott, C. D., & Maraia, R. J., 1979. Gap heating with pressure gradients. In: *14th AIAA Thermophysics Conference*, AIAA Paper 79-1043, Orlando, FL.
- [9] Smith, D. M., Petley, D. N., Edwards, C. L. W., & Patten, A. B., 1983. An investigation of gap heating due to stepped tiles in zero pressure gradient regions of the shuttle orbiter thermal protection system. In: *21st AIAA Aerospace Sciences Meeting and Exhibit*, AIAA Paper 83-0120, Reno, NV.

- [10] Avery, D. E., Kerr, P. A., & Wieting, A. R., 1983. Experimental aerodynamic heating to simulated shuttle tiles. NASA TM-84654.
- [11] Petley, D. H., Smith, D. M., Edwards, C. L. W., Carlson, A. B., & Hamilton II, H. H., 1984. Surface step induced gap heating in the shuttle thermal protection system. *Journal of Spacecraft and Rockets*, vol. 11, pp. 156–161.
- [12] Avery, D. E., 1985. Experimental aerodynamic heating to simulated shuttle tiles in laminar and turbulent boundary layers with variable flow angles at a nominal Mach number of 7. NASA TP-2307.
- [13] Hunt, L. R., & Notestine, K. K., 1990. Aerodynamic pressure and heating-rate distributions in tile gaps around chine regions with pressure gradients at a Mach number of 6.6. NASA TP-2980.
- [14] Charbonnier, J., & Boerrigter, H., 1993. Contribution to the study of gap induced boundary layer transition in hypersonic flow. In: *AIAA/DGLR 5th International Aerospace Planes and Hypersonics Technologies Conference*, AIAA Paper 93–5111, Munich, Germany.
- [15] Grotowsky, M. G., & Ballmann J., 2000. Numerical investigation of hypersonic step-flows. *Shock Waves*, vol. 10, pp. 57–72.
- [16] Paolicchi, L. T. L. C., & Santos, W. F. N., 2018. Length-to-depth ratio effects on aerodynamic surface quantities of a hypersonic gap flow. *AIAA Journal*, vol. 56, pp. 780–792.
- [17] Leite, P. H. M., & Santos, W. F. N., 2019. Computational analysis of a rarefied hypersonic flow over backward-facing steps. *Journal of Thermophysics and Heat Transfer*, vol. 33, pp. 749–761.
- [18] Palharini, R. C., & Santos, W. F. N., 2019. The impact of the length-to-depth ratio on aerodynamic surface quantities of a rarefied hypersonic cavity flow. *Aerospace Science and Technology*, vol. 88, pp. 110–125.
- [19] Leite, P. H. M., & Santos, W. F. N., 2015. Computational analysis of the flow field structure of a non-reacting hypersonic flow over forward-facing steps. *Journal of Fluid Mechanics*, Vol. 763, pp. 460–499.
- [20] Bird, G. A., 1994. *Molecular Gas Dynamics and the Direct Simulation of Gas Flows*, Oxford University Press, Oxford, England, UK.
- [21] Roohi, E., & Stefanov, S., 2016. Collision partner schemes in DSMC: From micro/nano flows to hypersonic flows. *Physics Reports*, vol. 656, pp. 1–38.
- [22] Bird, G. A., 1981. Monte Carlo simulation in an engineering context. In: *Progress in Astronautics and Aeronautics: Rarefied gas Dynamics*, edited by Sam S. Fisher, vol. 74, part I, pp. 239–255, AIAA New York.
- [23] Bird, G. A., 1989. Perception of numerical method in rarefied gasdynamics. In: *Rarefied gas Dynamics: Theoretical and Computational Techniques*, edited by E. P. Muntz, and D. P. Weaver and D. H. Campbell, vol. 118, Progress in Astronautics and Aeronautics, AIAA, New York, pp. 374–395.
- [24] Borgnakke, C. & Larsen, P. S., 1975. Statistical collision model for Monte Carlo simulation of polyatomic gas mixture. *Journal of Computational Physics*, vol. 18, pp. 405–420.
- [25] Boyd, I. D., 1998. Analysis of rotational nonequilibrium in standing shock waves of nitrogen. *AIAA Journal*, vol. 28, pp. 1997–1999.
- [26] Bird, G. A., 2009. A comparison of collision energy-based and temperature-based procedures in DSMC. In: *26th International Symposium on Rarefied Gas Dynamics*, edited by T. Abe, American Institute of Physics, pp. 245–250.

- [27] Alexander, F. J., Garcia, A. L., & Alder, B. J., 1998. Cell size dependence of transport coefficient in stochastic particle algorithms. *Physics of Fluids*, vol. 10, pp. 1540–1542.
- [28] Alexander, F. J., Garcia, A. L., & Alder, B. J., 2000. Erratum: cell size dependence of transport coefficient is stochastic particle algorithms. *Physics of Fluids*, vol. 12, pp. 731–731.
- [29] Chen, H., Zhang, B., & Liu, H., 2019. On the particle discretization in hypersonic nonequilibrium flows with the direct simulation Monte Carlo method. *Physics of Fluids*, vol. 31, pp. 076102.
- [30] Gorji, H., Kuchlin, S., & Jenny, P., 2019. Particle number control for direct simulation Monte-Carlo methodology using kernel estimates. *Physics of Fluids*, vol. 31, pp. 062008.
- [31] Sun, Z.-X., Tang, Z., He, Y.-L., & Tao, W.-Q., 2011. Proper cell dimension and number of particles per cell for DSMC. *Computers & Fluids*, vol. 50, pp. 1–9.
- [32] Garcia, A. L., & Wagner, W., 2000. Time step truncation error in direct simulation Monte Carlo. *Physics of Fluids*, vol. 12, pp. 2621–2633.
- [33] Hadjiconstantinou, N. G., 2000. Analysis of discretization in the direct simulation Monte Carlo. *Physics of Fluids*, vol. 12, pp. 2634–2638.
- [34] Kim, H. D., & Setoguchi, T., 2007. Shock-induced boundary layer separation. In: *8th International Symposium on Experimental and Computational Aerothermodynamics of Internal Flows*, Lyon, France.
- [35] Deepak, N. R., Gai, S. L. & Neely, A. J., 2010. A Computational study of high enthalpy flow over a rearward facing step. In: *8th AIAA Aerospace Sciences Meeting Including the New Horizons Forum and Aerospace Exposition*, AIAA Paper 2010–0444, Orlando, FL.